

Article

Design and Development of Explosion-Proof Cavity of Hydraulic System Power Unit Applied in Explosion-Proof Area

Hanzhe Chen ^{1,*}, Dingxuan Zhao ², Zhuxin Zhang ³, Tuo Jia ³, Ruoyu Zhao ⁴ and Zhengkun Qu ⁵¹ School of Mechanical and Aerospace Engineering, Jilin University, Changchun 130025, China² School of Mechanical Engineering, Yanshan University, Qinhuangdao 066000, China³ School of Vehicle and Energy, Yanshan University, Qinhuangdao 066000, China⁴ Process Planning Department, FAW Volkswagen, Changchun 130011, China⁵ Production Vehicle Manufacturing Department II, FAW Volkswagen, Changchun 130011, China

* Correspondence: hanzhechen_jlu@163.com

Abstract: The construction machinery and vehicles, especially the explosion-proof and explosion-isolation ability of the vehicles are playing an increasingly important role in the complex and unpredictable emergency rescue field. In this paper, the explosion-proof housing of hydraulic system power unit applied in engineering machinery is investigated, wherein the power unit includes motor, power supply and control element. Motor-driven hydraulic pump provides the necessary power for the hydraulic system. The gas explosion process, basic parameters, flame acceleration mechanism and the theory model of gas explosion in finite space are analyzed. Relevant mathematical models of the experimental gas explosion for explosion-proof cavity are established. Furthermore, the models are analyzed by numerical method. We simulate the dynamic process of explosion by software. The analysis, examination and simulation of structural strength are conducted on the explosion-proof cavity according to the maximum explosion pressure obtained from the simulation results. The reasonable design parameters satisfying the explosion-proof requirements are obtained. The explosion-proof cavity which is processed according to the design parameters is tested. The explosion-proof performance is verified by analyzing the experimental results. According to the test standard, the impact test, thermal test, pressure test, overpressure test and propagation test under internal ignition for the cavity are conducted. The results show that the pressure test coincides with the simulation results. The remaining test results also satisfy the experimental purpose. The reasonableness of the design of the explosion-proof cavity is verified, which can meet the actual requirements of the equipment.

Keywords: explosion-proof cavity; gas explosion; numerical method; explosion simulation; explosion-proof test



Citation: Chen, H.; Zhao, D.; Zhang, Z.; Jia, T.; Zhao, R.; Qu, Z. Design and Development of Explosion-Proof Cavity of Hydraulic System Power Unit Applied in Explosion-Proof Area. *Processes* **2022**, *10*, 1824. <https://doi.org/10.3390/pr10091824>

Academic Editors: Lijian Shi, Kan Kan, Fan Yang, Fangping Tang and Wenjie Wang

Received: 9 August 2022

Accepted: 31 August 2022

Published: 9 September 2022

Publisher's Note: MDPI stays neutral with regard to jurisdictional claims in published maps and institutional affiliations.



Copyright: © 2022 by the authors. Licensee MDPI, Basel, Switzerland. This article is an open access article distributed under the terms and conditions of the Creative Commons Attribution (CC BY) license (<https://creativecommons.org/licenses/by/4.0/>).

1. Introduction

This paper focuses on the design and development of the explosion-proof cavity of the hydraulic system power unit of the engineering machinery applied in the explosion-proof area. The reasonableness and reliability of the design, as well as its qualification for actual requirements, are verified by simulation and experiments.

In the conventional developing process, the performance of explosion-proof equipment needs to be verified by field tests. The performance of the equipment cannot be guaranteed before the test, which will prolong the design period and increase the developing cost. Therefore, it is not a reasonable and economical way to verify the explosion-proof performance by direct test. Researchers have established many mathematical models by studying the shape of solid obstructions [1], premixed obstructions [2], adiabatic wall circular tubes and connected vessels on the combustion influential conditions [3,4]. Although many researchers have conducted experiments through numerical simulation, most of the

experimental results feature defects and deviations from the actual situation [5,6]. In this research, the explosion process is simulated, and the explosion power is quantitatively analyzed, which makes it possible to create the appropriate explosion-proof design of the equipment in advance, so as to achieve the maximum benefit of the design [7].

In order to qualify the explosion-proof cavity, which is designed based on the standard requirements, the experimental explosion process in the cavity is numerically simulated and analyzed. The maximum pressure of the internal explosion is obtained from the simulation [8,9] and the theoretical model of heat exchange between gas and wall during gas combustion [10,11]. Then, the strength of the cavity is analyzed. The simulation and analysis can shorten the design period of the explosion-proof cavity and reduce the cost of testing in a reasonable way.

2. Explosion Model and Simulation Principle

2.1. Integral Structure of Explosion-Proof Cavity

According to the basic size of the motor, we design the power switch and circuit board of the explosion-proof cavity and the standard requirements for the actual equipment in the environment. The explosion-proof cavity is 850 mm long, 224 mm wide, 150 mm tall. The base plate is 10 mm thick, cover plate 12 mm thick, support plate for motor 60 mm thick, and the remaining plates are 20 mm thick. Figure 1 is an axonometric drawing of three-dimensional structure of explosion-proof cavity.

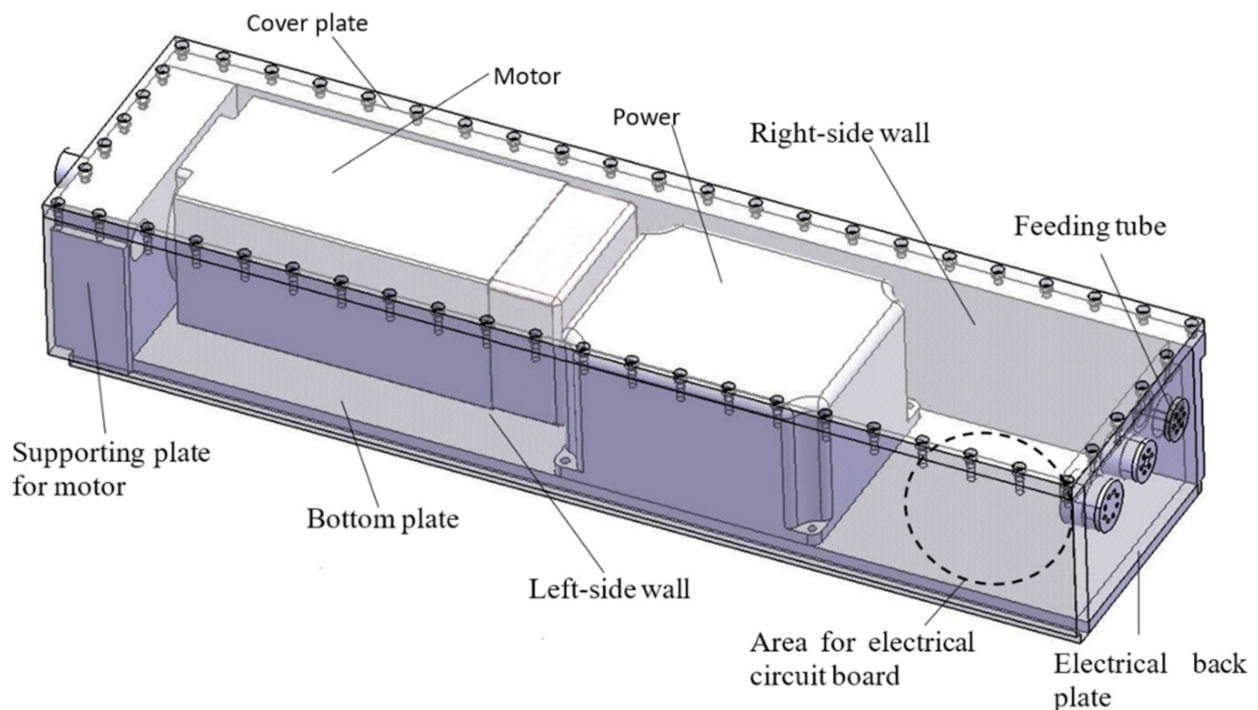


Figure 1. Axonometric Drawing of Three-dimensional Structure of Explosion-proof Cavity.

The construction of the cavity has a critical impact on the gas explosion. The cavity width of the gas explosion wave attenuation characteristics of the impact is particularly significant, so the construction of the explosion-proof cavity should focus on the construction and size of the cavity [12,13].

In this cavity, the plane joint surface is mainly the joint surface of the box and the cover plate, and the joint surface of the motor stopper and the motor support plate. In order to arrange the screw position reasonably, the length of the joint surface is chosen as 20 mm because the joint surface of the box and the cover is connected by screws.

In the main control box, in addition to the above-mentioned plane joint surface, there is another important joint surface, which is the motor shaft joint surface. The minimum length of the motor shaft joint surface is 12.5 mm, and the maximum clearance is 0.20 mm. Considering the rotation of the motor shaft and the machining process of the joint surface, the width of the motor shaft joint surface is 25 mm, and the maximum clearance is 0.30 mm [14,15].

2.2. Basic Theory of Gas Explosion

2.2.1. Selection of Explosive Gas

In general, there are four forms of gas explosions, including constant pressure combustion, deflagration, explosive blast, and constant volume combustion.

According to the possible working environment analysis of the explosion-proof cavity and the requirements in GB 3836-2, the explosion gas hazard grade and category of explosion-proof cavity is confirmed to be IIB class. The ethylene is selected as the explosive mixture for the experiment. Additionally, the volume ratio of air under atmospheric pressure is $8 \pm 0.5\%$ [16,17].

Constant-volume combustion is an ideal process. In practice, simultaneous ignition cannot be achieved. The general combustion situation is from a local ignition and then diffusion to the whole device. Due to the very fast diffusion, such a situation can be idealized as fixed-volume combustion [18,19].

2.2.2. Theoretical Model of Gas Explosion in Finite Space

The processes of explosion and its transmission are complex, and they involve combustion, thermodynamics, hydrodynamics and kinetics of the chemical reaction. With the development of computing science and technology, numerical simulation technology has been used more and more in the area of combustible gas explosion. The accuracy and reliability of numerical simulation is improved gradually, so that more accurate mathematical expressions can be established to analyze the explosion process.

Normally, the explosion model itself is already quite cumbersome, and it is only possible to obtain a clear analytical solution under specific assumptions. Until now, the main three models that can be recognized have been isothermal explosion model, adiabatic explosion model and general model [20–22].

However, these three models are derived from the thermodynamic point of view from the start, not considering the fluid dynamics and the chemical reaction kinetics in the explosion process. The three models cannot fully simulate the explosion process, and the analytical solution obtained is also relatively coarse, greatly limiting its scope of application. With the development of numerical theory, more precise mathematical expressions can be established for the analysis of the explosion process [23–25].

2.2.3. Basic Parameters of Gas Explosion

The main parameters affecting combustible gas explosion include: combustion velocity, flame velocity, adiabatic flame temperature, constant volume explosion pressure, explosion pressure rising rate, explosion strength eigenvalue, ignition energy and ignition temperature.

When the concentration of fuel is 6.5%, the adiabatic flame temperature of the ethylene mixture is 2380K.

Expression of Constant volume explosion pressure value:

$$P_f = P_i \cdot \frac{n_f T_f}{n_i T_i} \quad (1)$$

where, P , n , T represent pressure, quantity in mole and temperature, i represents the initial state and f is the final state of the reaction.

Expression of Explosion Pressure Rising rate:

$$\left(\frac{dP}{dt}\right)^{\frac{1}{3}} \text{constant}_{G_{max}} \quad (2)$$

where K_G is the gas explosion value (unit: Pa·m/s), This parameter can evaluate the explosion power and dangerousness.

E_{min} is the minimum energy that can cause gas explosion, referred to as threshold value, and is the parameter describing the sensitivity of gas ignition.

2.2.4. Flame Acceleration Mechanism

The feedback process of combustion velocity and turbulence of the flame are shown in Figure 2.

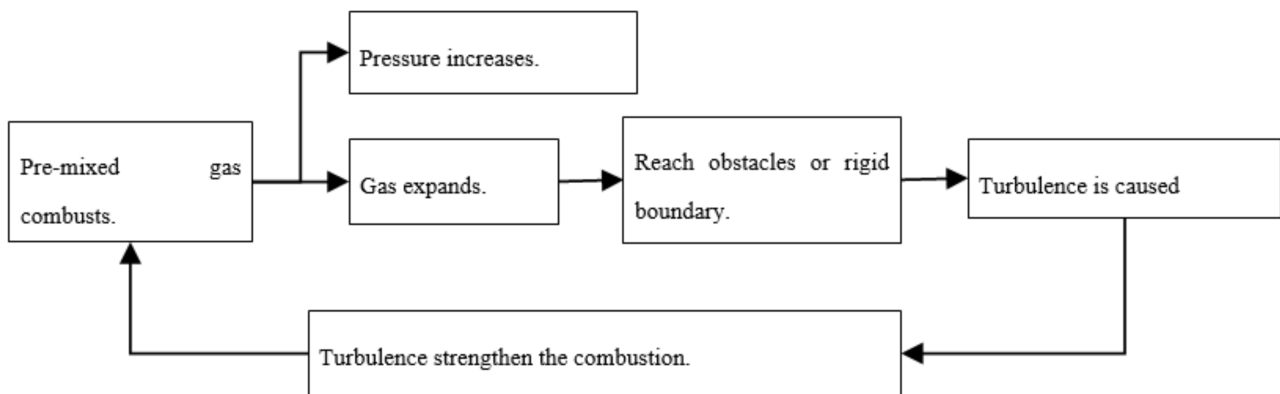


Figure 2. Schematic diagram of the feedback effect of combustion velocity and turbulence.

2.3. Establishment of Gas Explosion Model in Explosion-Proof Cavity

2.3.1. Physical Model

Essentially, gas explosion is a fast-transmission combustion process, which is transmitted by the flame produced in the process of igniting the local gas from the ignition source. The process has a strong chemical reaction on the interface between the burned gas and unburned gas, leading to the transformation of material and energy. The physical model of combustion can be idealized as shown in Figure 3.

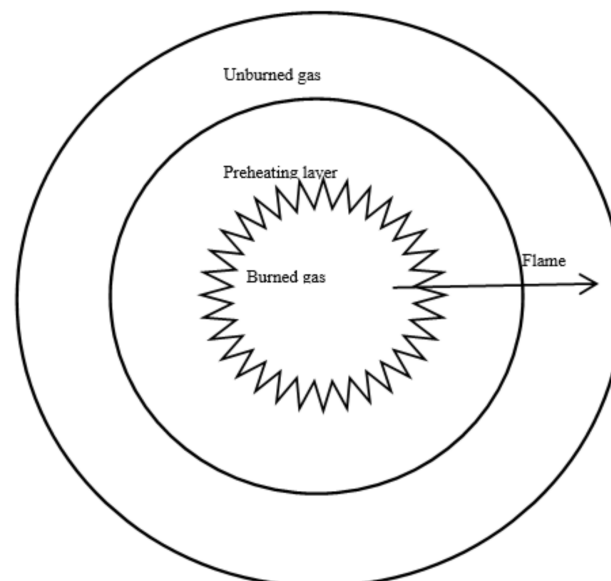


Figure 3. Physical model of combustion in spherical container.

The cross section of explosion-proof cavity is rectangular, and the ignition position can be any point within the cavity. There are great differences between the rectangular and spherical combustion model. The rectangular one is more complex, because the height of the motor and power in explosion-proof cavity are almost the same as the inner cavity of explosion-proof cavity. The two-dimensional model is simplified from the cross section which includes an ignition source. As shown in Figure 4, regardless of the influence exerted by the edge of the box on the explosion, the combustion process inside the explosion-proof cavity is modeled as the following diagram.

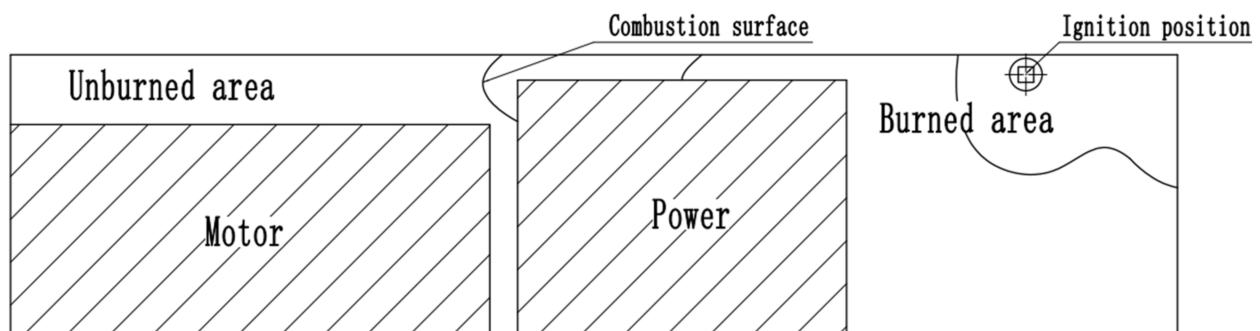


Figure 4. Physical Model of Combustion in Explosion-proof Cavity.

2.3.2. Mathematical Model

The actual explosion model of the explosion-proof cavity is quite complicated. In order to create a numerical simulation, the explosion process of the explosion-proof cavity is simplified based on the follow assumptions:

- (a) The explosive gas mixture in the explosion-proof cavity has been mixed evenly and remained stationary before ignition;
 - (b) The gas in the explosion-proof cavity is actual gas, which satisfies the actual state equation of the gas;
 - (c) The explosion process of the mixed gas is an irreversible process with single proceeding;
 - (d) The specific heat capacity of the mixed gas varies as temperature changes, which should adopt an interpolation method in calculation;
 - (e) Explosion-proof cavity is an adiabatic container, regardless of the heat exchange between the inside and outside of the explosion-proof cavity, including the heat exchange on the wall surface of the shell.
- (1) Basic equation

N-S equations are averaged by the Reynolds Method. The turbulence in the combustion process are described by using RNG K-epsilon turbulence model, so as to realizing the closure of the equations.

Equation of Mass Conservation:

$$\frac{\partial \rho}{\partial t} + \frac{\partial \rho u_i}{\partial x_i} = 0 \quad (3)$$

Equation of Conservation of Momentum:

$$\begin{aligned} \frac{\partial \rho u_i}{\partial t} + \frac{\partial}{\partial x_i} \left(\rho u_i u_j - \mu_e \frac{\partial u_i}{\partial x_j} \right) \\ = - \frac{\partial p}{\partial x_i} + \frac{\partial}{\partial x_j} \left(\mu_e \frac{\partial u_j}{\partial x_j} \right) - \frac{2}{3} \cdot \frac{\partial}{\partial x_j} \left[\delta_{ij} \left(\rho k + \mu_e \frac{\partial u_k}{\partial x_k} \right) \right] \end{aligned} \quad (4)$$

Equation Energy Conservation:

$$\frac{\partial \rho h}{\partial t} + \frac{\partial}{\partial x_j} \left(\rho u_j h - \frac{\mu_e}{\sigma_h} \cdot \frac{\partial h}{\partial x_j} \right) = \frac{Dp}{Dt} + S_h \quad (5)$$

Equation of Conservation of Chemical Composition:

$$\frac{\partial(\rho Y_{fu})}{\partial t} + \frac{\partial}{\partial x_j} \left(\rho u_j Y_{fu} - \frac{\mu_e}{\sigma_{fu}} \cdot \frac{\partial Y_{fu}}{\partial x_j} \right) = R_{fu} \quad (6)$$

The two-dimensional model is divided into x and y directions, and the above Equations (3)–(6) are expressed as follows:

$$\frac{\partial \rho}{\partial t} + \frac{\partial \rho u}{\partial x} + \frac{\partial \rho v}{\partial y} = 0 \quad (7)$$

$$\begin{cases} \frac{\partial(\rho u)}{\partial t} + \frac{\partial}{\partial x} \left(\rho u^2 - 2\mu_e \frac{\partial u}{\partial x} \right) + \frac{\partial}{\partial y} \left(\rho v u - \mu_e \frac{\partial u}{\partial y} - \mu_e \frac{\partial v}{\partial y} \right) \\ = -\frac{\partial p}{\partial y} - \frac{2}{3} \cdot \frac{\partial}{\partial x} \left[\rho k + \mu_e \left(\frac{\partial u}{\partial x} + \frac{1}{y} \frac{\partial(yv)}{\partial y} \right) \right] \\ \frac{\partial(\rho v)}{\partial t} + \frac{\partial}{\partial x} \left(\rho u v - \mu_e \frac{\partial u}{\partial x} - \mu_e \frac{\partial v}{\partial x} \right) + \frac{\partial}{\partial y} \left(\rho v^2 - 2\mu_e \frac{\partial v}{\partial y} \right) \\ = -\frac{\partial p}{\partial y} - \frac{2}{3} \cdot \frac{\partial}{\partial x} \left[\rho k + \mu_e \left(\frac{\partial u}{\partial x} + \frac{1}{y} \frac{\partial(yv)}{\partial y} \right) \right] \end{cases} \quad (8)$$

$$\begin{aligned} & \frac{\partial(\rho h)}{\partial t} + \frac{\partial}{\partial x} \left(\rho u h - \frac{\mu_e}{\sigma_h} \cdot \frac{\partial h}{\partial x} \right) + \frac{\partial}{\partial y} \left(\rho v h - \frac{\mu_e}{\sigma_h} \cdot \frac{\partial h}{\partial y} \right) \\ & = \frac{Dp}{Dt} + \sigma_{xx} \frac{\partial u}{\partial x} + \sigma_{yy} \frac{\partial v}{\partial y} + \mu_e \left(\frac{\partial u}{\partial y} + \frac{\partial v}{\partial x} \right)^2 \end{aligned} \quad (9)$$

where:

$$\begin{aligned} \sigma_{xx} &= 2\mu_e \frac{\partial u}{\partial x} - \frac{2}{3} \cdot \mu_e \left[\frac{1}{y} \cdot \frac{\partial(yv)}{\partial y} + \frac{\partial u}{\partial x} \right] \\ \sigma_{yy} &= 2\mu_e \frac{\partial v}{\partial y} - \frac{2}{3} \cdot \mu_e \left[\frac{1}{y} \cdot \frac{\partial(yv)}{\partial y} + \frac{\partial u}{\partial x} \right] \\ & \frac{\partial(\rho Y_{fu})}{\partial t} + \frac{\partial}{\partial x} \left(\rho u Y_{fu} - \frac{\mu_e}{\sigma_{fu}} \cdot \frac{\partial Y_{fu}}{\partial x} \right) \\ & + \frac{\partial}{\partial y} \left(\rho v Y_{fu} - \frac{\mu_e}{\sigma_{fu}} \cdot \frac{\partial Y_{fu}}{\partial y} \right) = R_{fu} \end{aligned} \quad (10)$$

where U and V refer to the speeds of x and y directions, respectively.

In Equations (7)–(10), the two-dimensional model in the explosion-proof cavity is expressed as the following general Equation(11).

$$\frac{\partial(\rho \varphi)}{\partial t} + \frac{\partial}{\partial x} \left(\rho u \varphi - \Gamma_\varphi \frac{\partial \varphi}{\partial x} \right) + \frac{\partial}{\partial y} \left(\rho v \varphi - \Gamma_\varphi \frac{\partial \varphi}{\partial y} \right) = S_\varphi \quad (11)$$

where φ , Γ_φ , S_φ , respectively, represent the general physical quantity, effective transport coefficient and the source item.

(2) Turbulence Model

In order to increase the calculation efficiency, the RNG k - ε model is used to calculate the complex situations which satisfies the turbulent in the explosion-proof cavity. The k equation of the turbulent kinetic energy and the ε equation of turbulent dissipation ratio are shown as follows:

$$\begin{aligned} & \frac{\partial(\rho k)}{\partial t} + \frac{\partial(\rho k u_i)}{\partial x_i} \\ & = \frac{\partial}{\partial x_j} \left[\left(\alpha_k \mu_{eff} \right) \cdot \frac{\partial k}{\partial x_j} \right] + G_k + G_b - \rho \varepsilon - Y_M \end{aligned} \quad (12)$$

$$\begin{aligned} & \frac{\partial(\rho \varepsilon)}{\partial t} + \frac{\partial(\rho \varepsilon u_i)}{\partial x_i} = \frac{\partial}{\partial x_j} \left[\left(\alpha_\varepsilon \mu_{eff} \right) \cdot \frac{\partial \varepsilon}{\partial x_j} \right] \\ & + C_{1\varepsilon} \cdot \frac{\varepsilon}{k} (G_k + C_{3\varepsilon} G_b) - C_{2\varepsilon} \rho \frac{\varepsilon^2}{k} - R_i \end{aligned} \quad (13)$$

$$\mu_{eff} = \mu + \mu_t \quad (14)$$

$$\mu_t = \rho C_\mu \frac{k^2}{\varepsilon} \quad (15)$$

where:

ρ —fluid density;

μ —fluid dynamic viscosity;

μ_t —turbulence viscosity, $\mu_t = \rho C_\mu \frac{k^2}{\varepsilon}$;

C_μ —constant, the value is 0.09, empirical constant (=0.09);

G_k —turbulence kinetic energy caused by average velocity gradient, which is calculated in

$$G_k = \mu_t \left(\frac{\partial u_i}{\partial x_j} + \frac{\partial u_j}{\partial x_i} \right) \cdot \frac{\partial u_i}{\partial x_j}$$

G_b —the turbulence generated by the influence of buoyancy, $G_b = \beta g_i \cdot \frac{\mu_t}{Pr_t} \cdot \frac{\partial T}{\partial x_i}$, Pr_t refers

to Prandtl number of turbulence, $Pr_t = \frac{\mu C_p}{k}$ represents the component of the gravitational

acceleration in i direction, β is the coefficient of thermal expansion, which can be calculated

$$\text{in } \beta = -\frac{1}{\rho} \cdot \frac{\partial \rho}{\partial T};$$

Y_M —The effect of compressible turbulent expansion on the total dissipation rate, calculated

by $Y_M = 2\rho\varepsilon M_t^2$, M_t is the Mach number of turbulence, M_t refers to local sound velocity,

$$a = \sqrt{\gamma RT};$$

$C_{1\varepsilon}$, $C_{2\varepsilon}$, $C_{3\varepsilon}$ are empirical constants, taking the values of 1.44, 1.92, 0.09, respectively;

σ_k , σ_ε are the Prandtl numbers corresponding to the turbulent kinetic energy and turbulent dissipation rate, taking the values of 1.0 and 1.3, respectively.

α_k , α_ε are the reciprocals of the effective Prandtl numbers of turbulent kinetic energy and turbulent energy dissipation rate.

(3) Combustion model

To simplify the reaction mechanism, assuming that the reaction is an irreversible process with single proceeding, the combustion reaction equation of ethylene in the explosion-proof cavity is expressed as follows:



According to the actual condition of the explosion-proof cavity, the gas explosion in the explosion-proof cavity is simulated by the laminar finite velocity/eddy dissipation model.

In the turbulent combustion zone of laminar finite velocity/eddy dissipation model, the rate of chemical reaction is mainly reflected in fragmentation rate of each gas parcel, and the rate value depends on the lower value of the gas parcel fragmentation rate of the burned gas and the unburned gas, which are expressed as (17)–(19):

$$R_i = -\min[R_{i,A}, R_{i,T}] \quad (17)$$

$$R_{i,A} = \left| B\rho^2 Y_1 Y_2 \exp\left(-\frac{E}{RT}\right) \right| \quad (18)$$

$$R_{i,T} = C_{EBU} \rho \frac{\varepsilon}{k} \min(Y_1, Y_2, Y_3) \quad (19)$$

where:

B —pre-exponential factor;

E —activation energy;

R —Planck constant for gas;

$R_{i,A}$ —burning rate of laminar reaction;

$R_{i,T}$ —combustion velocity of turbulence;

C_{EBU} —empirical constant, taking value from 0.34–0.4;

Y_1 , Y_2 , Y_3 correspond to the mass fraction of fuel, oxygen and combustion products, respectively.

(4) Wall function

The influence of wall on flow model can be solved by wall function. The function can simulate the explosion model in the box with the RNG k- ϵ model.

In order to describe the viscous bottom, transition layer of the wall area, the transition layer and the three sub-regions of the logarithmic law layer, two dimensionless parameters u^+ and y^+ are introduced, respectively representing the speed and distance.

$$u^+ = \frac{u}{\left(\frac{\tau_w}{\rho}\right)^{\frac{1}{2}}} \quad (20)$$

$$y^+ = \frac{\Delta y \cdot \rho \left(\frac{\tau_w}{\rho}\right)^{\frac{1}{2}}}{\mu} \quad (21)$$

where:

u —the average speed of the fluid in an hour;

τ_w —avoiding shear stress;

Δy —the distance from each point to the wall.

The wall function is a semi empirical formula derived from the analysis and experiment. Experimental studies show that the near wall region can be divided into three layers, and the place closest to the wall is called the viscous sublayer, and the flow is the layer in the flow state, molecular viscosity plays a decisive role in momentum, heat and mass transport. The core area becomes a completely turbulent layer flow plays a decisive role. The bottom region between the complete turbulence and the laminar bottom layer is the buffer layer the viscosity and turbulence of internal molecules play an important role.

For most of the high Reynolds number flow problems, the wall functional approach can be used to save computational resources. If the problem we study is a low Reynolds number flow problem, we need a suitable model that can be solved all the way to the wall, then we can choose a near-wall model for the solution. A law can be obtained according to a large amount of data, as shown in Figure 5, and each point in the graph represents the conclusion drawn from each experiment.

When $y^+ < 5$, it is considered to be a viscous bottom, where the velocity is distributed in a linear way along the normal distance of the wall:

$$u^+ = y^+ \quad (22)$$

When $5 < y^+ < 60$, it is considered to be a transitional layer because this layer is thin, and it is often classified into a logarithmic law layer in engineering.

When $60 < y^+ < 300$, it is considered to be a logarithmic law layer, in which the velocity is assumed to be distributed in a logarithmic way along the normal direction of the wall, namely:

$$u^+ = \frac{1}{\kappa} \ln y^+ + B = \frac{1}{\kappa} \ln(Ey^+) \quad (23)$$

where κ is a constant, B and E are constants related to the roughness of the wall surface.

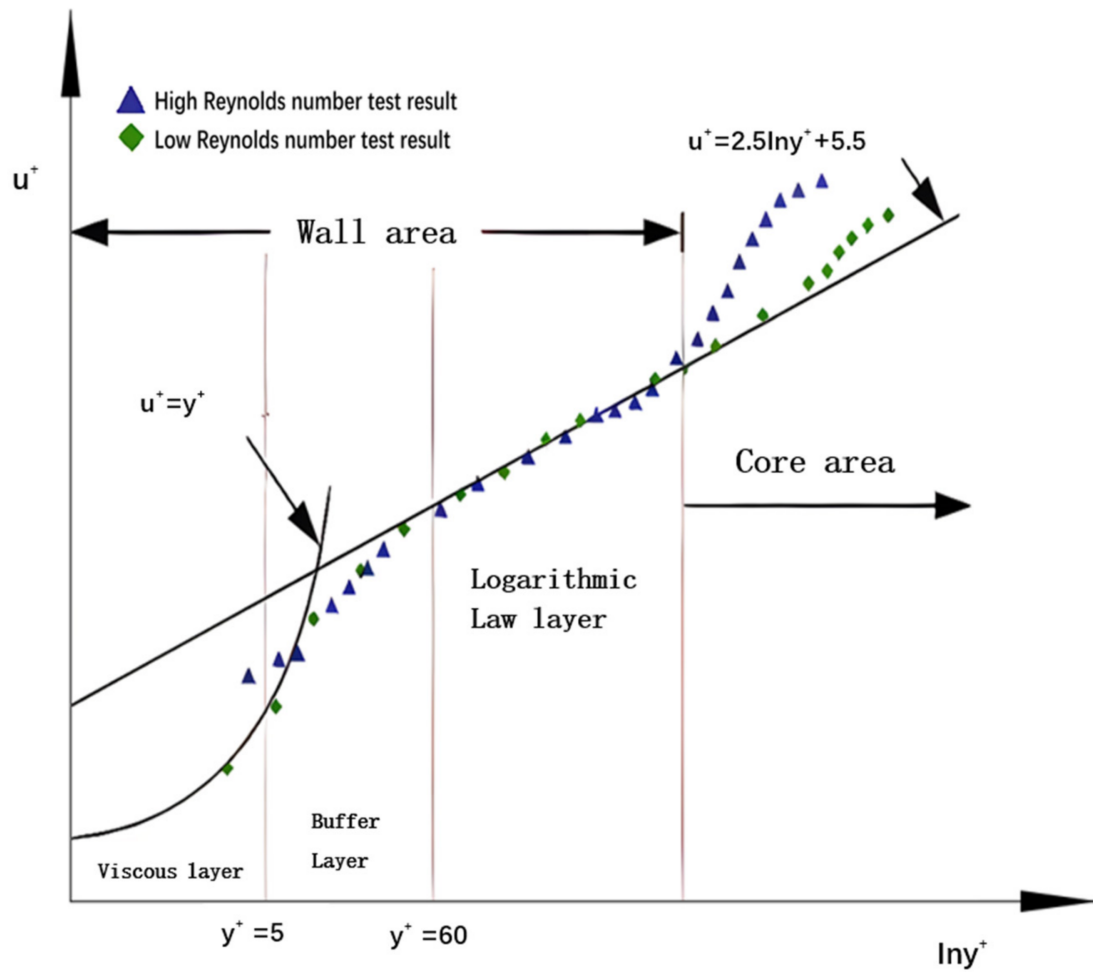


Figure 5. Wall function.

Assuming a node Δy_p away from the wall, the calculation formula for y^+ and τ_w is:

$$y^+ = \frac{\Delta y_p \left(C_p^{\frac{1}{4}} k_p^{\frac{1}{2}} \right) \rho}{\mu} \quad (24)$$

$$\tau_w = \rho C_p^{\frac{1}{4}} k_p^{\frac{1}{2}} u_p / u^+ \quad (25)$$

where, the subscript p refers to the relative physical quantity at the node p .

2.3.3. Numerical Method

When adopting the finite volume method, the mathematical model in explosion-proof cavity can be expressed as general Equation(11).

Taking central point P as representative, the general formula is integrated in the aspect of time and space. Additionally, N, S, W, E in Figure 6 refer to the upper, lower, left and right boundary points of the main grid, respectively. The dotted line indicates the boundary line that controls volume.

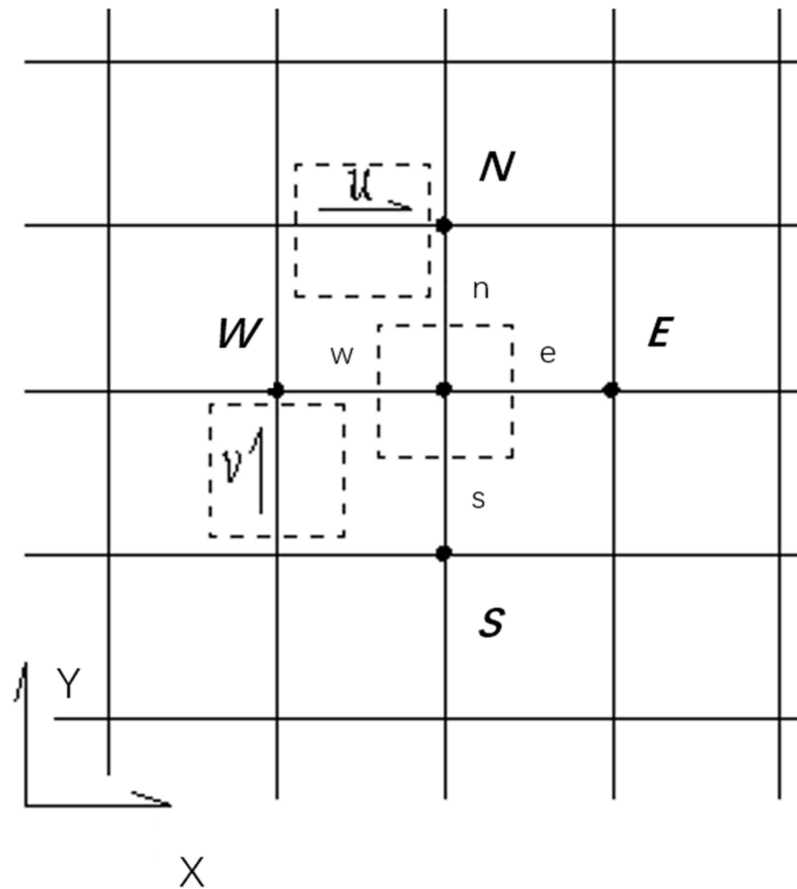


Figure 6. Schematic diagram of the two-dimensional grid.

In the control volume where P is taken as central point, the general Equation (11) is discretized into algebraic equations in each volume. We can acquire the following by linearization:

$$a_P \phi_P = a_N \phi_N + a_S \phi_S + a_W \phi_W + a_E \phi_E + b \quad (26)$$

where $a_P = a_N + a_S + a_W + a_E + (F_e - F_w) + (F_n - F_s) + a_P^0 - S_P \Delta V$, $a_N = D_n + \max(0, -F_n)$, $a_S = D_s + \max(0, F_s)$, $a_E = D_e + \max(0, -F_e)$, $a_W = D_w + \max(0, F_w)$, $b = S_C \Delta V + a_P^0 \phi_P^0$, $a_P^0 = \frac{\rho_P^0 \Delta V}{\Delta t}$; $F_n = (\rho u)_n \Delta x$, $F_s = (\rho u)_s \Delta x$, $F_e = (\rho u)_e \Delta y$, $F_w = (\rho u)_w \Delta y$; $D_n = \frac{\Gamma_n \Delta x}{(\Delta y)_n}$, $D_s = \frac{\Gamma_s \Delta x}{(\Delta y)_s}$, $D_e = \frac{\Gamma_e \Delta y}{(\Delta x)_e}$, $D_w = \frac{\Gamma_w \Delta y}{(\Delta x)_w}$.

(1) Separation Solution

The discrete equation is solved with the method of separation. The specific process is shown as follows:

- (a) Based on the current solution, to update the parameters of the fluid, especially in the first calculation, to update the value of the parameter with the initial solution;
- (b) In order to solve the value of u and v , solve the momentum equation of each direction successively based on the quality flow and current pressure of surface;
- (c) The obtained values of u and v can satisfy the continuity equation need to be verified first. If it cannot, derive the Poisson equation from the continuity equation and the linear momentum equation, and solve the values of pressure and velocity in the equation at the same time;
- (d) To solve the energy, turbulence and other parameters by using the derived values;
- (e) To verify whether the result is convergent. If not, repeat the above steps and obtain the convergence conditions.

(2) PISO Algorithm

The PISO algorithm is chosen to solve the pressure coupling equation. The iterative flowchart for PISO algorithm is shown in Figure 7 below. The p^* means a fixed predicted value of pressure, and the p^{**} means a fixed predicted value of p^* . It's the same for μ , v and ϕ .

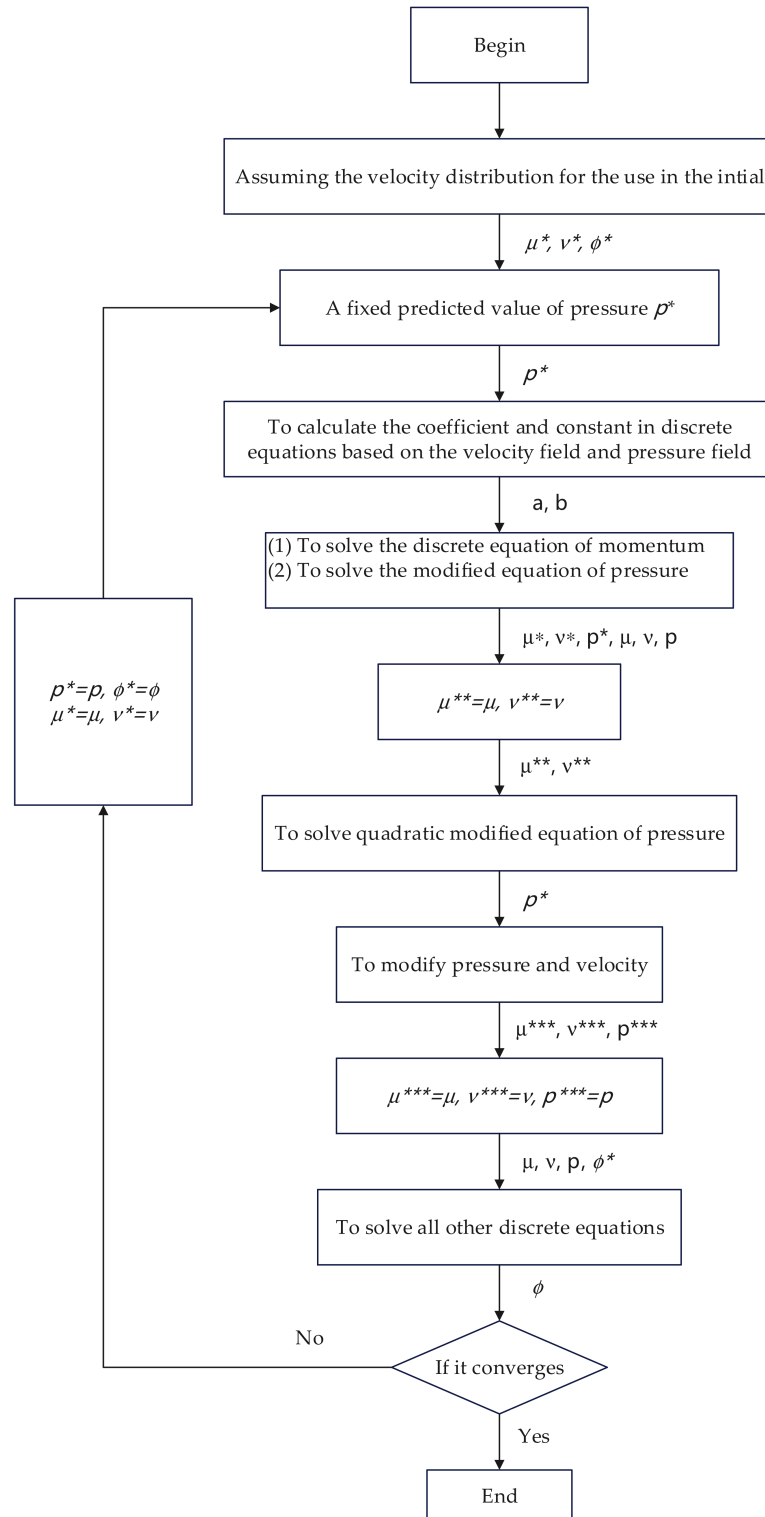


Figure 7. Flowchart of PISO Algorithm.

(3) Stability and convergence in the reaction flow

PISO algorithm converges in a high speed, which can be considered to converge in a certain range of values, with the convergence range of velocity and pressure is fixed within 0.001 and the range of energy set within 10^{-6} . In order to get the convergent solution quickly, and to ensure the stability of the solution process, under-relaxation method is used to guarantee the convergent solution according to the actual condition.

Equation (27) is a simplified under-relaxation equation where a is under-relaxation factor with value within (0, 1). It can take the value of 0.8, then find an appropriate value for a by experiment.

$$\varphi = \varphi_{old} + a\Delta\varphi \quad (27)$$

2.3.4. Initial and Boundary Conditions

The explosive mixed gas in the cavity is constituted by a certain proportion of ethylene and air. Regardless of CO_2 and H_2O in the air, in the initial state t_0 , the gas mixture is considered to be even and static, at this time, $T(t_0) = T_0$, $p(t_0) = p_0$, the velocity of x and y directions are 0.

In the initial state, the mass fraction of each mixed gas is: $m_{C_2H_4}(t_0) = 0.08$, $m_{O_2}(t_0) = 0.21$, $m_{N_2}(t_0) = 0.71$.

Due to the feature of explosion-isolation, the equipment cannot be an ignition source for external gas. Therefore, in this model, the wall is an adiabatic boundary, which means that the gas in the cavity has no heat exchange with outside.

In this case, $\frac{\partial\phi}{\partial y} = 0$ ($\phi = \rho(R, t), T(R, t), m_{fu}(R, t)$), $v(R, t) = 0$, $\frac{\partial T}{\partial n} = 0$, $\phi = 0$.

3. Simulation of Gas Explosion Process in Explosion-Proof Cavity

3.1. Strength Simulation of Explosion-Proof Cavity

An explosion combustion experiment on mixed ethylene gas in explosion-proof cavity is conducted. Figure 8 is the established two-dimensional model. Grid partitioning results are shown in Figure 9.

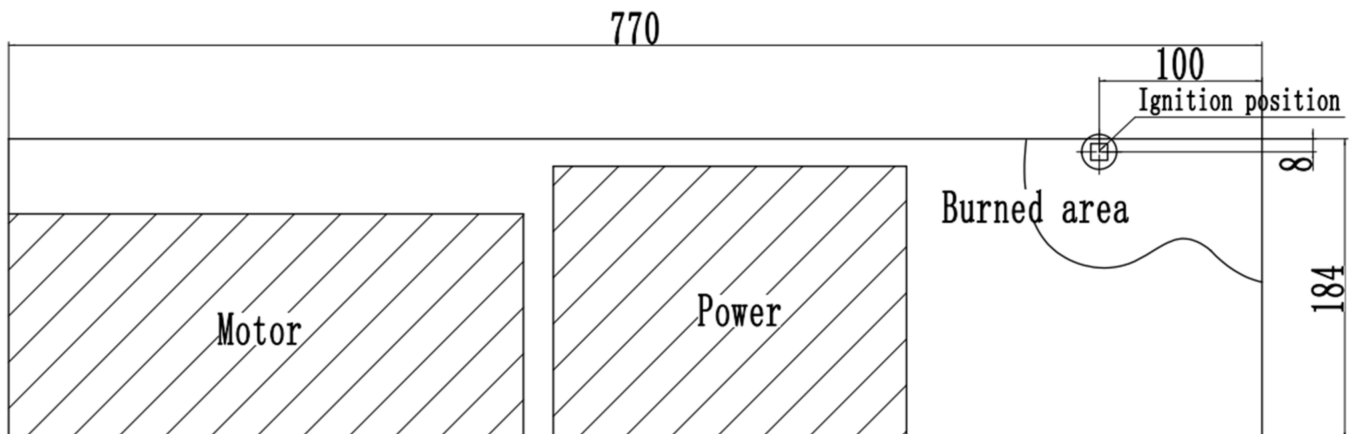


Figure 8. Two-dimensional model of explosion-proof cavity.

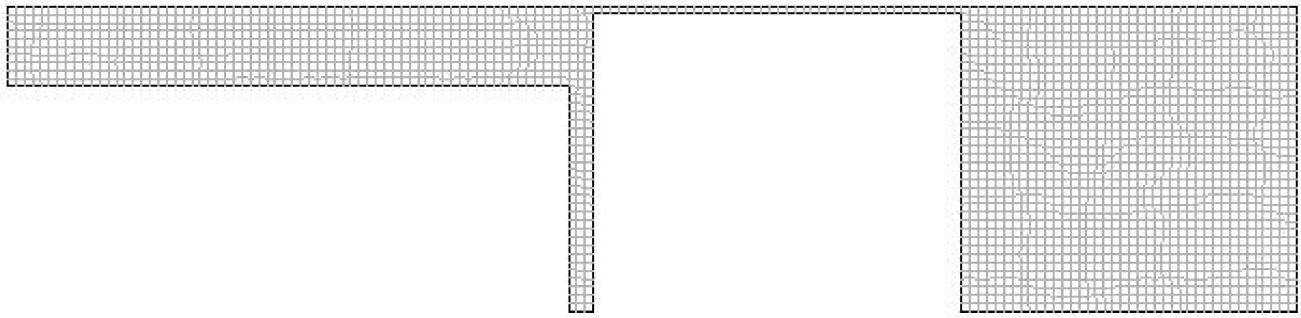


Figure 9. Grid partitioning results.

The initial condition of simulation is set up as the Table 1. The simulation time step takes the value of 0.0001 s. The calculation results are recorded at every 10 steps. Figure 10a–f, respectively, are diagrams showing the explosion pressure at 0.001 s, 0.002, 0.005 s, 0.01 s, 0.015 s and 0.02 s. Figure 11 is a diagram present the maximum explosion pressure variation in the box recorded under each time step. And the maximum explosion pressure in the box is 0.762 Mpa. For the convenience of calculation, the maximum explosion pressure will adopt $p_{max} = 0.8$ Mpa.

Table 1. Initial condition of simulation.

| Premixed Gas | Initial State of Gas | Initial Temperature (K) | Temperature of Ignition Source (K) | Wall State |
|------------------|----------------------|-------------------------|------------------------------------|-----------------|
| Ethylene and Air | Static | 300 | 2000 | Heat Insulation |

3.2. Strength Analysis of Explosion-Proof Cavity

According to the standards, hydrostatic load should be 1.5 times of the maximum explosion pressure. In the design of the explosion-proof cavity, the design strength of the bolt of the explosion-proof cavity cover plate can meet the requirement, while the other plates of the surface of the cavity take the method of full welding. The box is simplified as an integral for analysis. The cavity material is made of 316L stainless steel, with yield strength $\sigma_s = 310$ mpa, density $\rho = 7930$ kg/m³, elastic modulus $E = 1.95 \times 10^{11}$ Pa, Poisson's ratio $\mu = 0.3$. This is shown in Figure 12.

Afterwards, 1.2 MPa uniform distributed load is added to all surfaces of the box. The maximum stress of the cavity is shown in Figures 13 and 14.

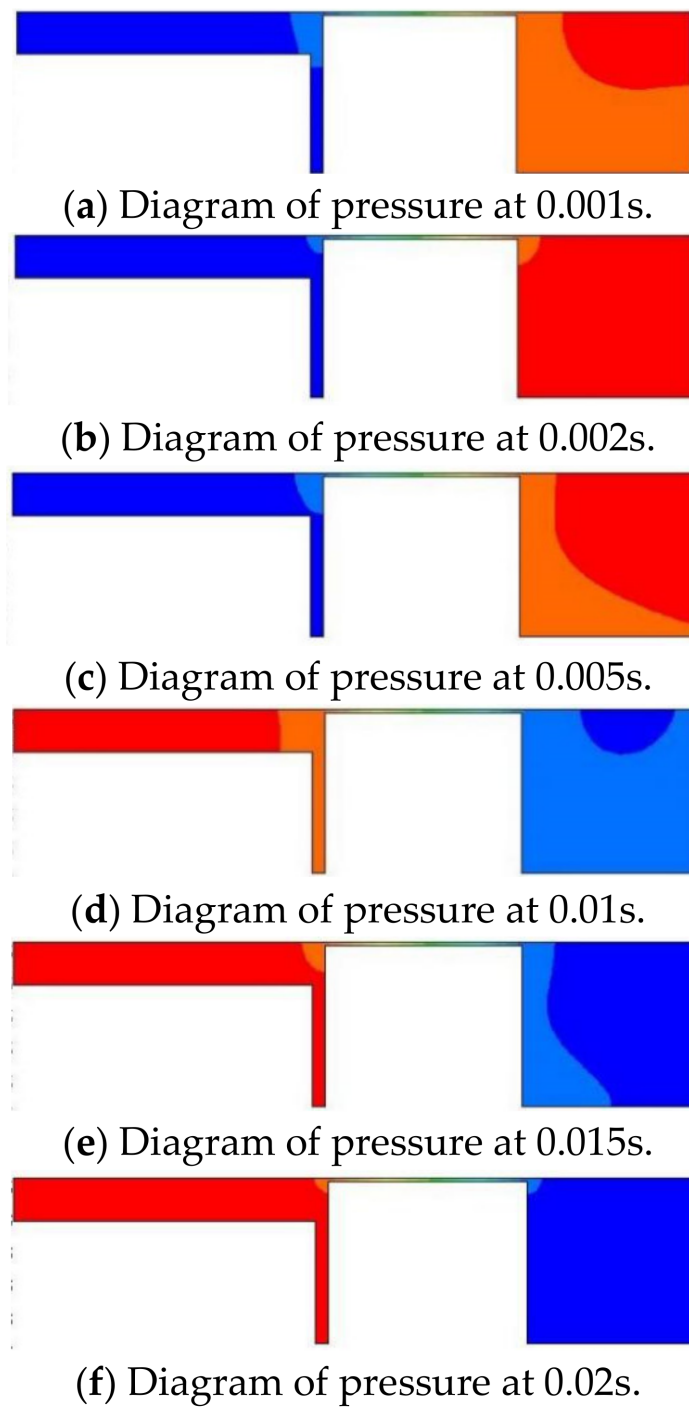


Figure 10. Diagram of pressure during explosion process.

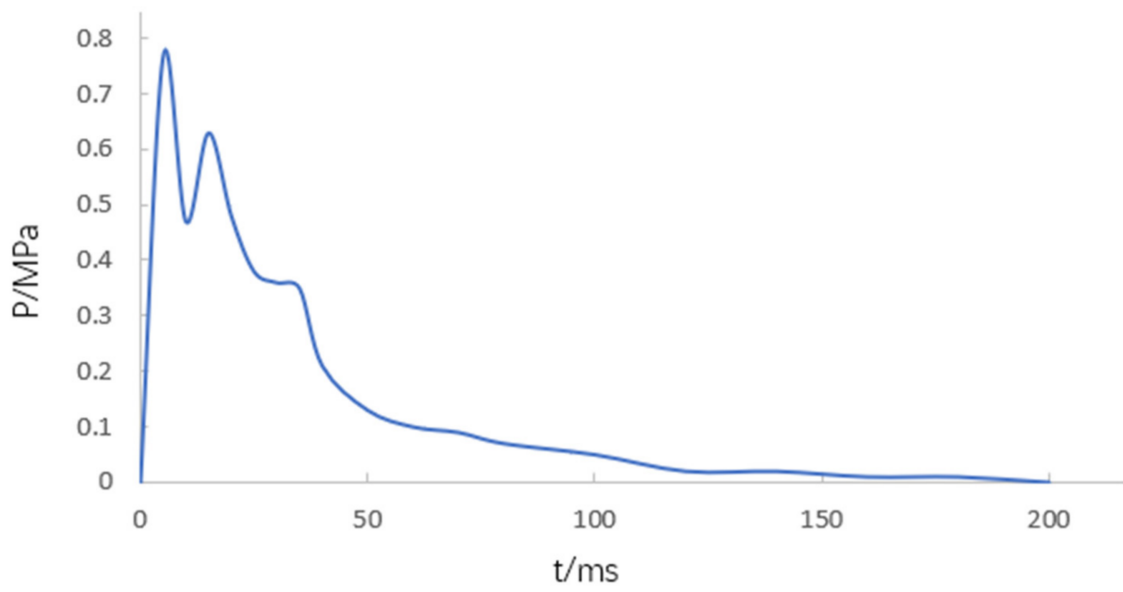


Figure 11. Diagram of maximum explosion pressure variation in the cavity.

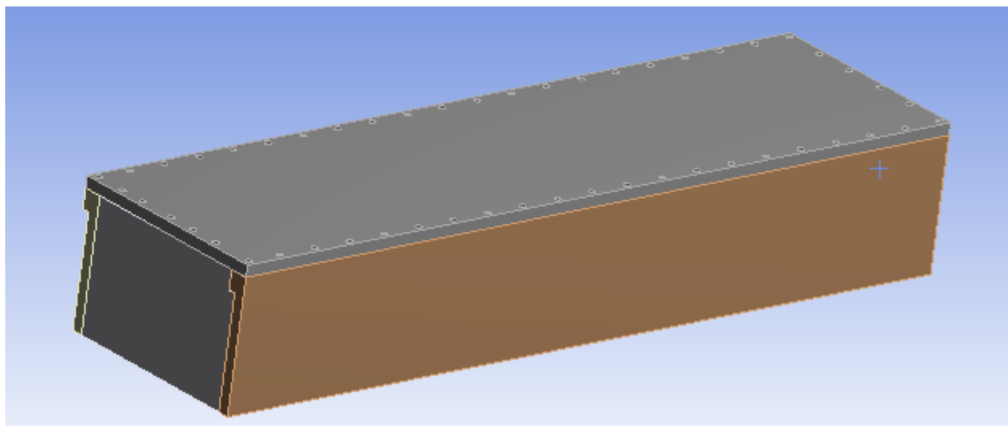


Figure 12. Simplified three-dimensional model of box.

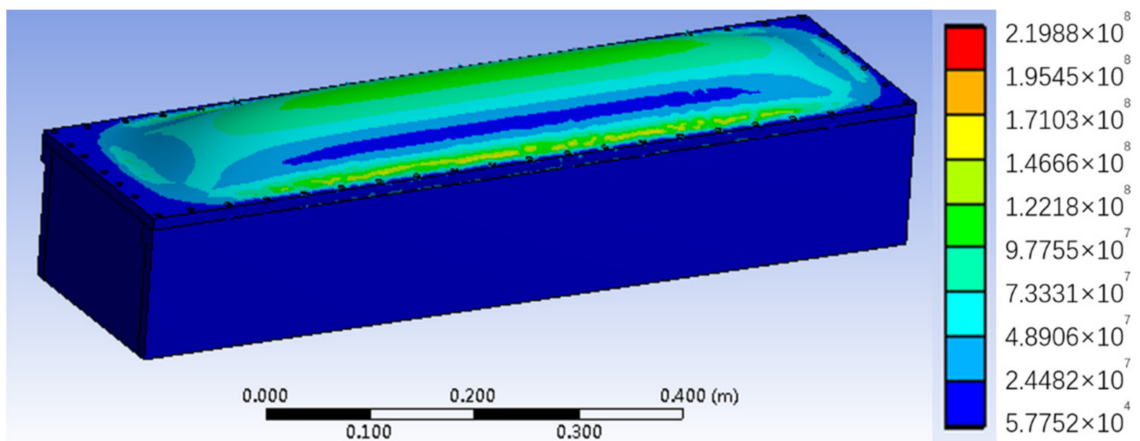


Figure 13. The maximum stress of the box.

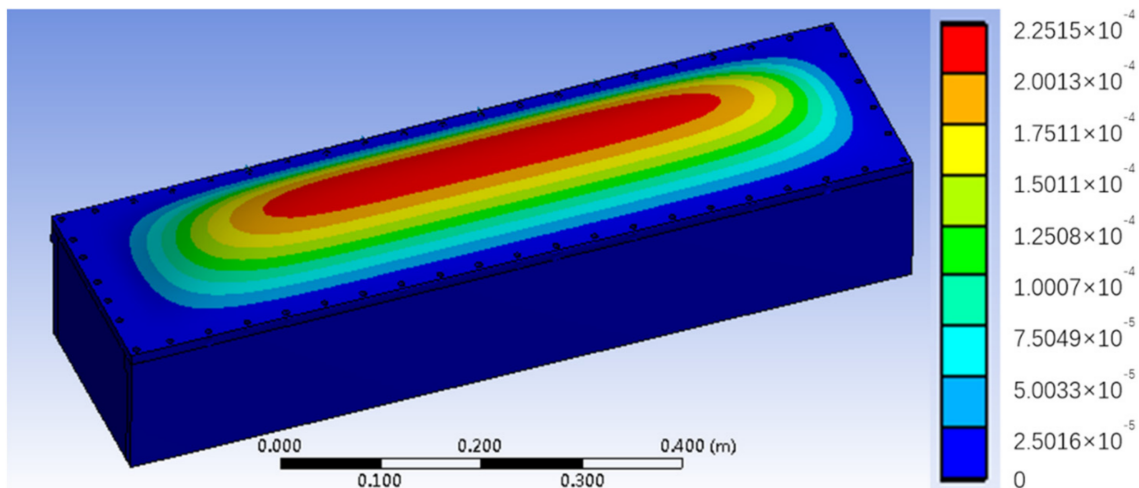


Figure 14. The maximum deformation of the box.

It can be seen from the analysis diagram that the explosion-proof cavity is subject to 1.2 MPa explosion force, with the maximum stress of 219.8 MPa, which is less than 310 MPa, the maximum displacement deformation of 0.225 mm. The results satisfy the design requirements.

4. Explosion-Proof Test

According to the requirements of “General Requirements for equipment” and “Equipment Protected by Explosion-isolation Housing “d” in Explosive Environment”, impact test, equipment thermal test, pressure test and propagation test under internal ignition on explosion-resistant cavity are performed to verify its explosion-proof performance.

4.1. Impact Test

In “General Requirements for equipment”, the equipment applied on explosion-proof cavity is classified as type II equipment, the test height of explosion-isolation shell of explosion-proof cavity is 0.7 m. The schematic diagram of the test device is shown in Figure 15.

The impact test should be conducted on a well-assembled equipment, the impact point of the test should be selected as the weakest point of the shell, and on the outside of the impact-bearing parts.

In the impact test, a number of surfaces of each explosion isolation chamber and the transparent parts of the test did not produce any damage, so the explosion isolation chamber impact test qualified.

According to the test records shown in Table 2, the test results of the impact test on explosion-proof cavity shell meet the requirements.

Table 2. Impact Test record of explosion-proof cavity shell.

| Test Sample | Height(m) | Result |
|-----------------|-----------|--------------------------|
| Cover plate | 0.7 | No damage on the surface |
| Left-side wall | 0.7 | No damage on the surface |
| Right-side wall | 0.7 | No damage on the surface |

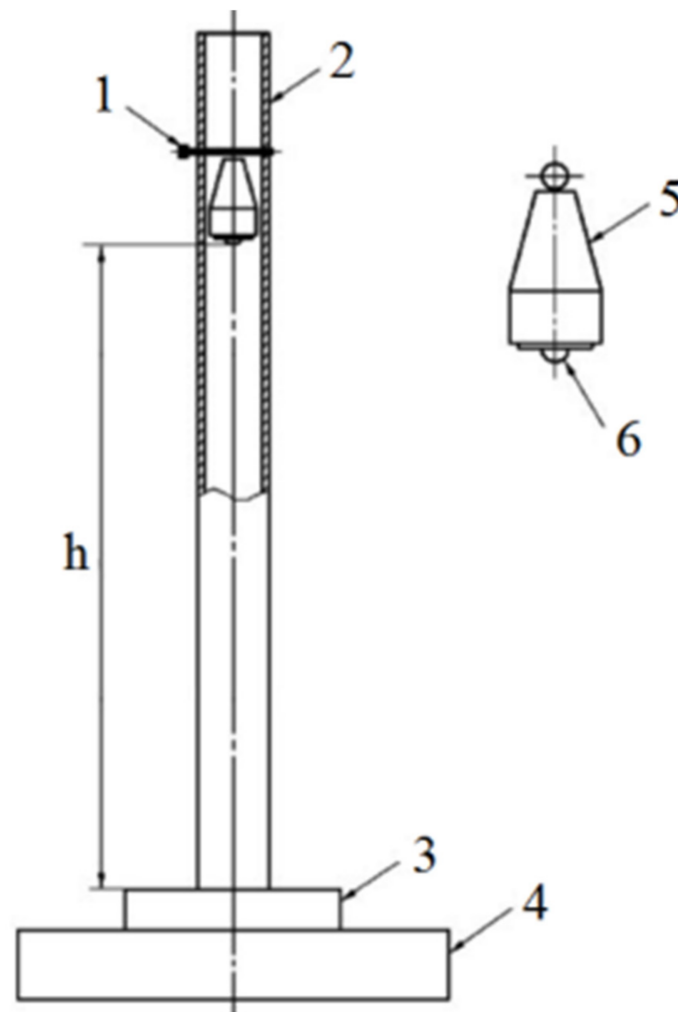


Figure 15. Schematic diagram of the testing equipment for impact test. 1. Bolt for adjusting height; 2. Tube; 3. Experimental sample; 4. Steel base (mass ≥ 20 kg); 5. Steel hammer block by quenching; 6. Hem-spherical steel punch by quenching of 25 mm diameter; h. Falling height.

4.2. Thermal Test

According to the standards, the equipment temperature group is T4, which means the maximum surface temperature cannot exceed 130 °C. In the thermal experiment, after the motor has worked for 45 min, the temperature of explosion-proof cavity reaches a stable state.

According to the recorded data shown in Table 3, it is known that the maximum surface temperature in the main control box is 45 °C, which is less than 130 °C, and the thermal test of the main control box is considered qualified.

Table 3. Thermal Test record of explosion-proof cavity shell.

| Testing Device | Working Hours (min) | Temperature of the Surface (°C) |
|----------------|---------------------|---------------------------------|
| Motor | 45 | 45 |

4.3. Pressure Test on Explosion-Proof Cavity

The static pressure method is chosen in the overpressure test of the explosion-proof cavity. According to the standards, the exerted pressure is 1.5 times the maximum internal explosion pressure. In this pressure test, the internal explosion pressure will be measured first, then we proceed to the overpressure test.

4.3.1. Preparation for Tests

The auxiliary hole of the explosion-proof cavity is arranged as in Figure 16. In the explosion-proof cavity, the gas input and output hole are arranged at both ends of the upper cover plate in order to ensure that the explosive mixed gas can fill the cavity, and two pressure measuring points are arranged at both ends of the side walls.

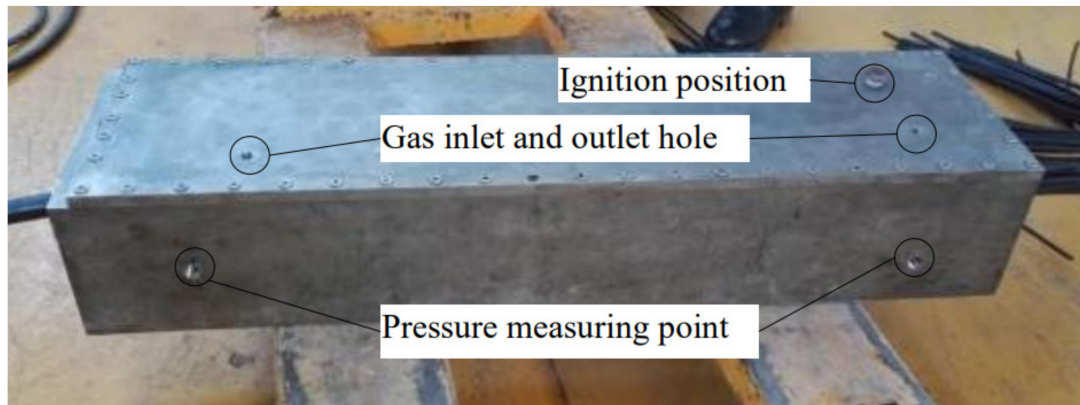


Figure 16. Layout of Test holes.

4.3.2. Measurement of Internal Explosion Pressure

Explosion pressure of explosion-proof cavity is measured during internal explosion. In the experiment, an explosion-proof experimental tank is selected, the schematic structure of which is shown in Figure 17.

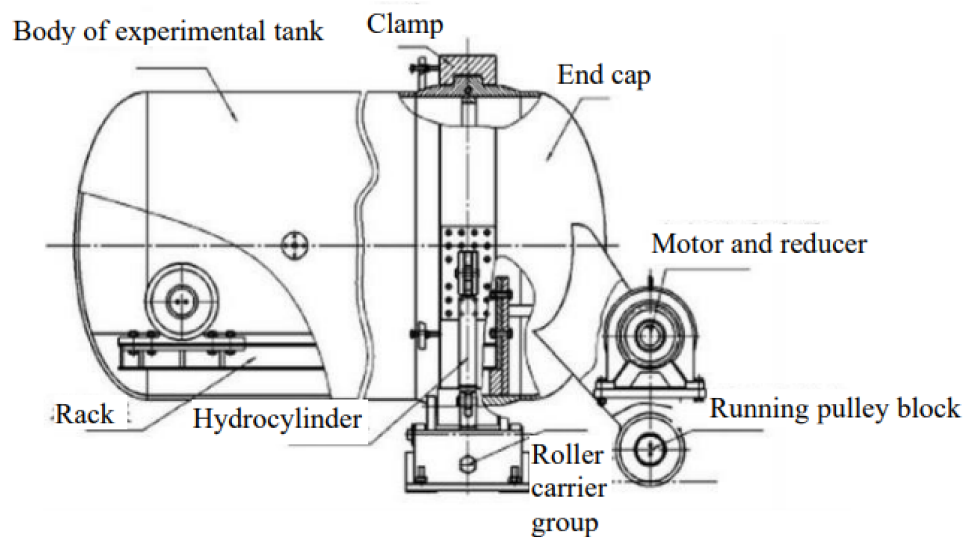


Figure 17. Schematic diagram of explosion-proof experimental tank structure.

The explosion-proof cavity is connected with a ventilation pipe, equipped with a fire plug and a pressure sensor. When connected, the experimental cavity is pushed into the experimental tank, and the end cap of the experimental tank is closed to test the pressure. Figure 18 is a connection diagram of experimental pipeline for explosion-proof cavities.

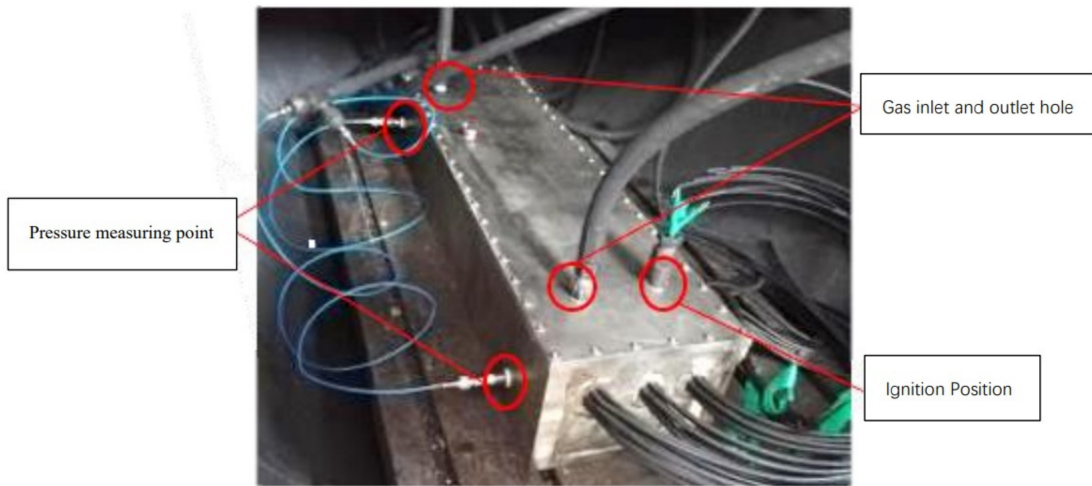
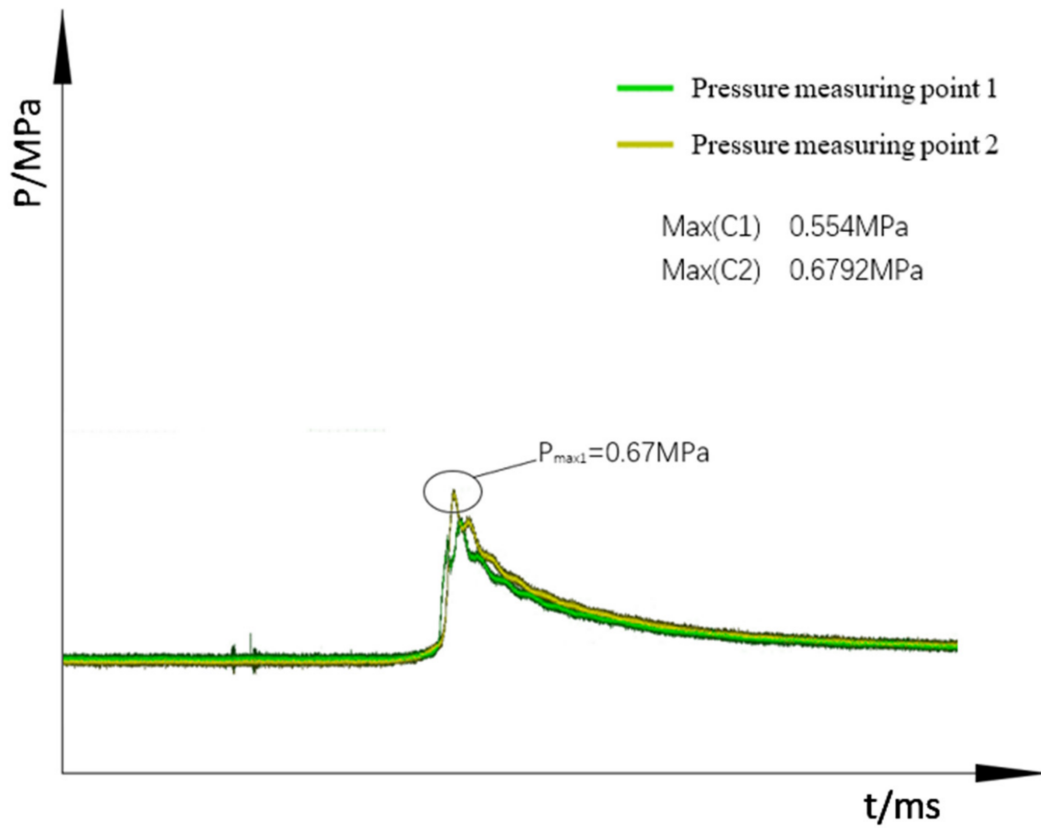


Figure 18. Connection diagram of experimental pipeline for explosion-proof cavities.

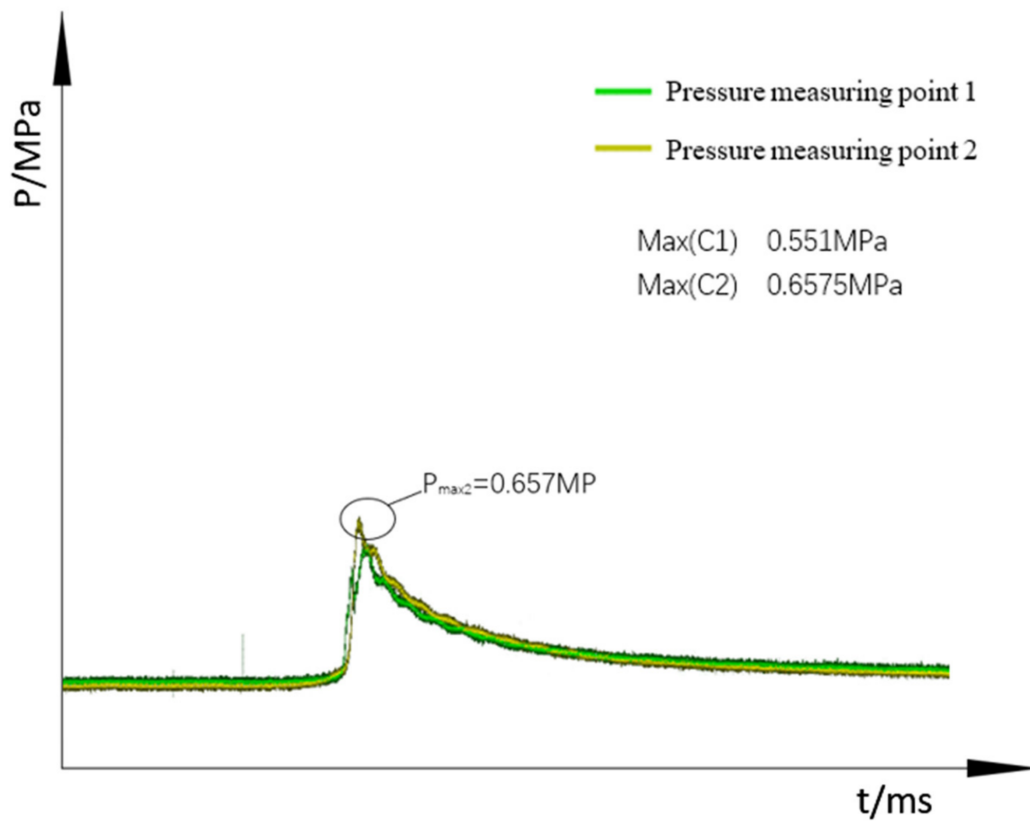
After gases inside explosion-proof cavity are fully mixed, the explosion-proof cavity is ignited for testing the explosion pressure inside the box. The curve of explosion pressure is recorded. According to the standards, the maximum pressure measured among three tests is the explosion pressure.

The test recorder recorded three test results as shown in Figure 19. Two curves in the diagram are the pressure curves measured at two pressure measuring points respectively.

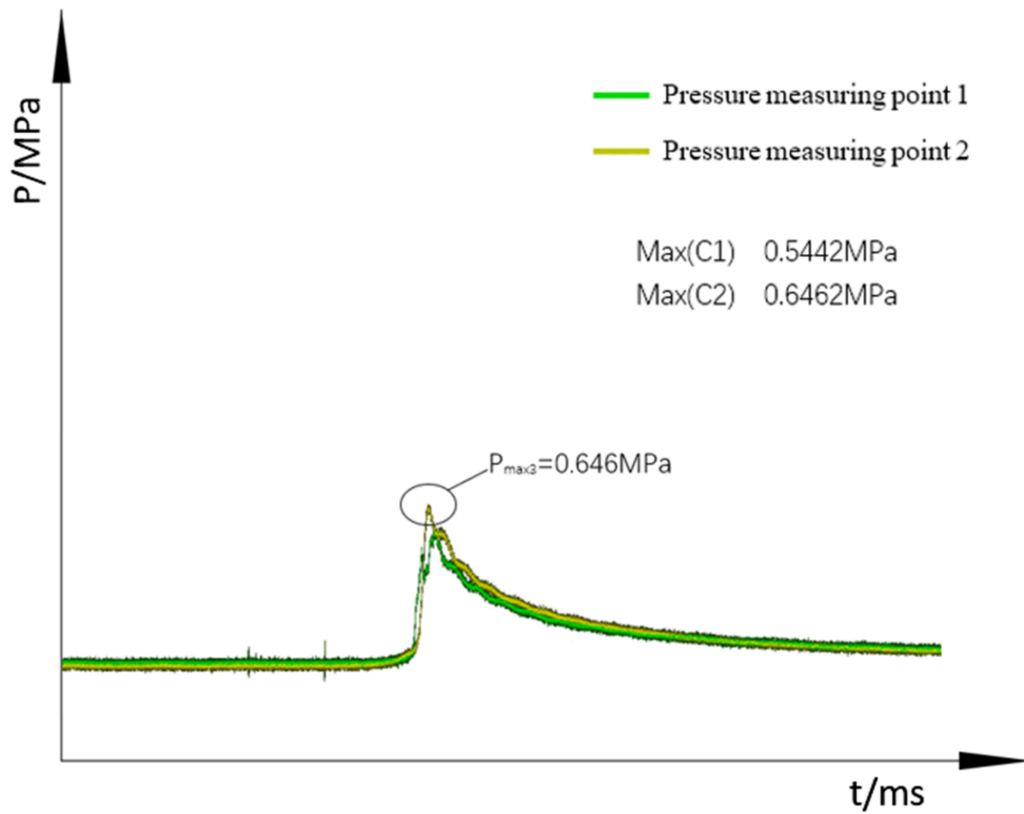


(a) The first result of the pressure test

Figure 19. Cont.



(b) The second result of the pressure test



(c) The third result of the pressure test

Figure 19. Results of the pressure test.

The maximum explosion pressure measured among three tests is 0.670 MPa. The simulation results are 0.762 MPa. Two results are close so the explosion simulation of explosion-proof cavity is considered to be reasonable.

4.3.3. Overpressure Test

According to the standards, hydrostatic pressure method is used in overpressure test. The exerted pressure should be 1.5 times the maximum internal explosion pressure. The condition shall be maintained for 10 s at such pressure value. The cavity will be considered to be qualified if no damage is caused during the test.

In the overpressure test on the explosion-proof cavity, the exerted pressure value is calculated as below: $1.5 \times 0.67 \text{ MPa} = 1.005 \text{ MPa}$.

The original air inlet of the explosion-proof cavity is directly used as water inlet hole. Additionally, joints and other experimental auxiliary holes are processed by sealing treatment. Asbestos pads are used as the seal for connecting surface. The testing setup is shown in Figure 20.



Figure 20. Testing setup of pressure test.

The water inlet of the hydraulic test desk is connected to the water inlet. When the pressure value shown on the pressure gauge reaches up to 1.005 MPa, the state is maintained for 10 s. Then, the valve is closed.

After the test, the explosion-proof cavity shows no damage and obvious deformation both inside and outside. The explosion-proof cavity is deemed to meet the requirements of overpressure test.

4.3.4. Propagation Test under Internal Ignition

As required, the ethylene gas of $8 \pm 0.5\%$ is prepared in the experimental tank and in the explosion-proof chamber. Propagation test under internal ignition is conducted for three times. After each test, the gas inside the experimental tank and explosion-proof cavity shall be exhausted and fed again.

In each test, no explosion occurred in the experimental tank, which proved that there was no propagation of explosion in the explosion-proof cavity. The cavity is deemed to be qualified.

4.4. Analysis of Experimental Results

During the experimental phase, we conducted the following four sets of tests. They are the Impact tests, the Equipment thermal tests, the Pressure tests and the Propagation tests.

According to the experimental results, the numerical simulation results are consistent with the experimental results, and the design parameters all meet the requirements of use. The numerical simulation from a new numerical idea is obtained, which is similar with the actual combustion situation. The experiments proved the feasibility of the kind of square-shaped explosion-proof cavity.

5. Conclusions

In this paper, by analyzing the basic processing, parameters of gas explosion, flame acceleration mechanism, and the theory model of gas explosion in finite space, we establish relevant mathematical models of the experimental gas explosion for explosion-proof cavity and analyze the models in a numerical way. The dynamic process of explosion by software is simulated. The analysis, examination and simulation of structural strength of are carried out on the explosion-proof cavity according to the maximum explosion pressure obtained from the simulation results. The reasonable design parameters satisfying the explosion-proof requirements are obtained.

The explosion-proof cavity, which is processed according to the design parameters, is tested. The experimental results verify the explosion-proof performance. According to the test standards, the impact test, thermal test, pressure test, overpressure test and propagation test under internal ignition for the cavity are performed. The pressure test results are coincidence with the simulation results. The remaining test results also satisfy the experimental purpose. The reasonableness of the design of explosion-proof cavity is verified, which can meet the actual requirements.

In this paper, while constructing the explosion-isolation model, we mainly discuss the mechanism of gas explosion, and propose a theoretical model of gas explosion in a limited space. We also design an explosion-proof device that has a safety and excellent anti-explosion effect. The device conducts the experimental verification. It provides an idea for proposing a more accurate gas explosion model, and it also lays the theoretical and experimental foundation for designing a safer explosion isolation device in the future.

Author Contributions: Conceptualization, H.C. and D.Z.; methodology; software; validation, H.C. and T.J.; formal analysis, T.J.; investigation, H.C.; resources, Z.Z.; data curation, H.C.; writing—original draft preparation, H.C.; writing—review and editing, T.J.; visualization, R.Z. and Z.Q.; supervision, T.J.; project administration, R.Z.; funding acquisition, H.C. All authors have read and agreed to the published version of the manuscript.

Funding: This research received no external funding.

Institutional Review Board Statement: Not applicable.

Informed Consent Statement: Not applicable.

Data Availability Statement: The datasets used and/or analyzed during the current study are available from the corresponding author on reasonable request.

Conflicts of Interest: The authors declare no conflict of interest.

References

1. Naamansen, P.; Baraldi, D.; Hjertager, B.H.; Solberg, T.; Cant, S. Solution adaptive CFD simulation of premixed flame propagation over various solid obstructions. *J. Loss Prevent. Proc. Ind.* **2002**, *15*, 189–197. [[CrossRef](#)]
2. Sarli, V.D.; Benedetto, A.D.; Russo, G.; Jarvis, S.; Hargrave, G.K. Large eddy simulation and PIV measurements of unsteady premixed flames accelerated by obstacles. *Flow Turbul. Combust.* **2009**, *83*, 227–250. [[CrossRef](#)]

3. Cui, Y.Y.; Wang, Z.R.; Ma, L.S.; Zhen, Y.Y.; Sun, W. Influential factors of gas explosion venting in linked vessels. *J. Loss Prevent. Proc. Ind.* **2017**, *46*, 108–114. [[CrossRef](#)]
4. Wang, Z.R.; Jiang, J.C.; Zheng, Y.Y. Numerical analysis of gas explosion process in linked vessels. *Chem. Eng.* **2006**, *34*, 13–16.
5. Dong, L.; Qi, Z.; Ma, Q.; Shen, S.; Chen, J.; Ren, S. Influence of built-in obstacles on unconfined vapor cloud explosion-ScienceDirect. *J. Loss Prevent. Proc. Ind.* **2016**, *43*, 449–456.
6. Masri, A.R.; Ibrahim, S.S.; Nehzat, N.; Green, A.R. Experimental study of premixed flame propagation over various solid obstructions. *Exp. Therm. Fluid Sci.* **2000**, *21*, 109–116. [[CrossRef](#)]
7. Yang, P.; Teng, H.; Jiang, Z.; Ng, H.D. Effects of inflow Mach number on oblique detonation initiation with a two-step induction-reaction kinetic model. *Combust. Flame* **2018**, *193*, 246–256. [[CrossRef](#)]
8. Jurca, A.M.; Ghiciei, E.; Paun, F. Modernization of the test method for non-sparking materials intended for use in explosive areas. *Environ. Eng. Manag. J.* **2019**, *18*, 847–852. [[CrossRef](#)]
9. Teng, H.H.; Jiang, Z.L. On the transition pattern of the oblique detonation structure. *J. Fluid Mech.* **2012**, *713*, 659–669. [[CrossRef](#)]
10. Zhang, H.O. GB team special type of explosion-proof battery power supply units and special-type battery requirements introduced. *Elec. Expl. Prot.* **2012**.
11. Bioche, K.; Vervisch, L.; Ribert, G. Premixed flame-wall interaction in a narrow channel: Impact of wall thermal conductivity and heat losses. *J. Fluid Mech.* **2018**, *856*, 5–35. [[CrossRef](#)]
12. Xu, D.; Mu, C.; Li, Z.; Zhang, W. Influence of cavity width on attenuation characteristic of gas explosion wave. *Shock Vib.* **2021**, *2021*, 6634754. [[CrossRef](#)]
13. Liu, W.; Mu, C.; Li, Z. Influence of cavity structure on gas explosion characteristics in coal mine. *Powd. Technol.* **2022**, *398*, 117084. [[CrossRef](#)]
14. Grov, A.; Opsvik, H.; Eckhoff, R.K. Effects of significant damage of flame gap surfaces in flameproof electrical apparatus on flame gap efficiency. *J. Loss Prevent. Process Ind.* **2011**, *24*, 552–557. [[CrossRef](#)]
15. Solheim, F.; Arntzen, B.J.; Eckhoff, R.K. Effect of rusting and mechanical damage of gap surfaces on efficiency of flame gaps in flameproof electrical apparatus. *Process Saf. Environ. Prot.* **2012**, *90*, 317–325. [[CrossRef](#)]
16. Zhang, Y.; Pan, Z.; Yang, J.; Chen, J.; Chen, K.; Yan, K.; He, M. Study on the suppression mechanism of (NH₄)₂CO₃ and SiC for polyethylene deflagration based on flame propagation and experimental analysis. *Powder Technol.* **2022**, *399*, 1. [[CrossRef](#)]
17. Zhang, L.; Li, J.; Xue, J.; Zhang, C.; Fang, X. Experimental studies on the changing characteristics of the gas flow capacity on bituminous coal in CO₂-ECBM and N₂-ECBM. *Fuel* **2021**, *291*, 120115. [[CrossRef](#)]
18. Tatman, B.J.; Rockwell, R.D.; Goynes, C.P.; Medaniel, J.C.; Donohue, J.M. Experimental study of vitiation effects on flameholding in a cavity flameholder. *J. Propul. Power.* **2013**, *29*, 417–423. [[CrossRef](#)]
19. Teng, H.; Ng, H.D.; Li, K.; Luo, C.; Jiang, Z. Evolution of cellular structures on oblique detonation surfaces. *Combust. Flame* **2015**, *162*, 470–477. [[CrossRef](#)]
20. Jo, Y.D.; Cowl, D.A. Flame growth model for confined gas explosion. *Process Saf. Prog.* **2010**, *28*, 141–146. [[CrossRef](#)]
21. Zhang, C.; Abedini, M. Time-history blast response and failure mechanism of RC columns using Lagrangian formulation. *Structures* **2021**, *34*, 3087–3098. [[CrossRef](#)]
22. Wang, Z.; Qiang, H. Mechanical properties of thermal aged HTPB composite solid propellant under confining pressure. *Def. Technol.* **2022**, *18*, 618–625. [[CrossRef](#)]
23. Zhang, L.; Huang, M.; Xue, J.; Li, M.; Li, J. Repetitive Mining Stress and Pore Pressure Effects on Permeability and Pore Pressure Sensitivity of Bituminous Coal. *Nat. Resour. Res.* **2021**, *30*, 4457–4476. [[CrossRef](#)]
24. Liu, W.; Liu, L.; Wu, H.; Chen, Y.; Zheng, X.; Li, N.; Zhang, Z. Performance analysis and offshore applications of the diffuser augmented tidal turbines. *Ships Offshore Struct.* **2022**, 1–10. [[CrossRef](#)]
25. Wang, Z.; Qiang, H.; Wang, J.; Duan, L. Experimental Investigation on Fracture Properties of HTPB Propellant with Circumferentially Notched Cylinder Sample. *Propellants Explos. Pyrotech.* **2022**, *47*, e202200046. [[CrossRef](#)]